nature chemistry

ARTICLES

PUBLISHED ONLINE: 11 NOVEMBER 2012 | DOI: 10.1038/NCHEM.1497

Stability of xenon oxides at high pressures

Qiang Zhu[1]*, Daniel Y. Jung[2], Artem R. Oganov[1,3]*, Colin W. Glass[4], Carlo Gatti[5] and Andriy O. Lyakhov[1]

Xenon, which is quite inert under ambient conditions, may become reactive under pressure. The possibility of the formation of stable xenon oxides and silicates in the interior of the Earth could explain the atmospheric missing xenon paradox. Using an *ab initio* evolutionary algorithm, we predict the existence of thermodynamically stable Xe–O compounds at high pressures (XeO, XeO_2 and XeO_3 become stable at pressures above 83, 102 and 114 GPa, respectively). Our calculations indicate large charge transfer in these oxides, suggesting that large electronegativity difference and high pressure are the key factors favouring the formation of xenon compounds. However, xenon compounds cannot exist in the Earth's mantle: xenon oxides are unstable in equilibrium with the metallic iron occurring in the lower mantle, and xenon silicates are predicted to decompose spontaneously at all mantle pressures (<136 GPa). However, it is possible that xenon atoms may be retained at defects in mantle silicates and oxides.

Xenon is a noble gas, and is chemically inert under ambient conditions. However, a few xenon fluorides have been identified[1–3] with xenon atoms in oxidation states +2, +4, +6 or +8. With application of high pressure, the molecular phase of insulating XeF_2 has been reported to transform into two- and three-dimensional extended solids and become metallic[4]. Clathrate Xe–H solids have also been observed at pressures above 4.8 GPa (ref. 5). Two xenon oxides—XeO_3 and XeO_4 (ref. 6)—have long been known to exist at ambient pressure, but are unstable and decompose explosively above 25 °C and −40 °C, respectively[7]. Moreover, a metastable crystalline XeO_2 phase with local square-planar XeO_4 geometry has recently been synthesized under ambient conditions[8].

There is growing evidence to suggest that noble gases, especially xenon, may become more reactive under pressure[9]. The formation of stable xenon oxides and silicates could explain the missing xenon paradox—the observation that the amount of xenon in the Earth's atmosphere is an order of magnitude less than it would be if all xenon were degassed from the mantle into the atmosphere[10]. One explanation for this deficit is that the xenon is largely retained in the mantle. In fact, it has been reported that a few weight percent of xenon can be incorporated into SiO_2 at elevated pressures and high temperatures[11,12]. A recent theoretical investigation has shown that no xenon carbides are stable up to at least 200 GPa (ref. 13), and an experimental and theoretical high-pressure study[14] found no tendency for xenon to form metal alloys with iron or platinum.

Here, we investigate the possible stability of xenon oxides using quantum-mechanical calculations of their energetics. As the structures of stable xenon oxides are not known experimentally, we calculate them using a recently developed evolutionary algorithm for the prediction of crystal structures[15,16]. We also analyse the chemical bonding of these exotic compounds.

We performed structure prediction simulations of the Xe–O system for the compositions of XeO, XeO_2, XeO_3 and XeO_4 at 5, 50, 100, 120, 150, 180, 200 and 220 GPa. Our calculations at 5 GPa yielded the lowest-enthalpy structures to always contain O_2 molecules, indicating the tendency for segregation of the elements; indeed, at 5 and 50 GPa, decomposition was found to be energetically favourable. This suggests that the observations of Sanloup *et al.*[11,12] at 0.7–10 GPa correspond to an entropically driven incorporation of xenon impurities into the structure of SiO_2, rather than enthalpically driven formation of a stoichiometric xenon silicate or oxide.

However, detailed calculations at and above 100 GPa found a number of oxides stable against decomposition into the constituent elements. The most promising structures and compositions were investigated further. The Gibbs free energies of formation of these oxides under conditions of high pressure and temperature are shown in Fig. 1. One can see that at 0 K and high P, XeO, XeO_2 and XeO_3 become thermodynamically stable. We also performed quasi-harmonic free-energy calculations with phonon spectra computed using the finite-displacement method[17] to assess the effect of temperature (Fig. 1b). The inclusion of thermal effects clearly does not bring any qualitative changes into the picture, and XeO, XeO_2 and XeO_3 also remain thermodynamically stable at high temperatures.

Figure 2d shows the enthalpy of formation of xenon oxides as a function of pressure. Below 83 GPa, all xenon oxides are unstable. At 83 GPa, XeO–$Pbcm$ becomes stable, followed by XeO_2–$P2_1/c$ above 102 GPa and XeO_3–$P4_2/mnm$ above 114 GPa. There is an interesting trend for the oxidation number of xenon to increase with increasing pressure.

A simple and clear analysis of chemical bonding can be carried out using the electron localization function, ELF[18]. ELF gives information about the valence electron configuration of an atom in a compound. States with closed-shell electron configurations (Xe^0, $5s^25p^6$ and Xe^{6+}, $5s^2$) will exhibit a spherical ELF distribution, whereas open-shell states (Xe^{2+} and Xe^{4+}) will not. For Xe^{2+}, one p-orbital is empty and the ELF will have a toroidal shape. Similarly, Xe^{4+} can be formed by removing electrons from two p-orbitals, and the ELF will show a two-lobe maximum corresponding to the shape of the lone p-electron pair.

The most stable structure of XeO at 100 GPa has space group $Pbcm$ and eight atoms in the unit cell. As shown in Fig. 2a, the

[1]Department of Geosciences, Department of Physics and Astronomy, Stony Brook University, Stony Brook, New York 11794-2100, USA, [2]Laboratory of Crystallography, Department of Materials, ETH Honggerberg, Zurich, Switzerland, [3]Geology Department, Moscow State University, 119992 Moscow, Russia, [4]High Performance Computing Center, Universität Stuttgart, 70550, Stuttgart, Germany, [5]Istituto di Scienze e Tecnologie Molecolari del CNR (CNR-ISTM) e Dipartimento di Chimica, Universita' di Milano, via Golgi 19, 20133 Milan, Italy. *e-mail: qiang.zhu@stonybrook.edu; artem.oganov@stonybrook.edu

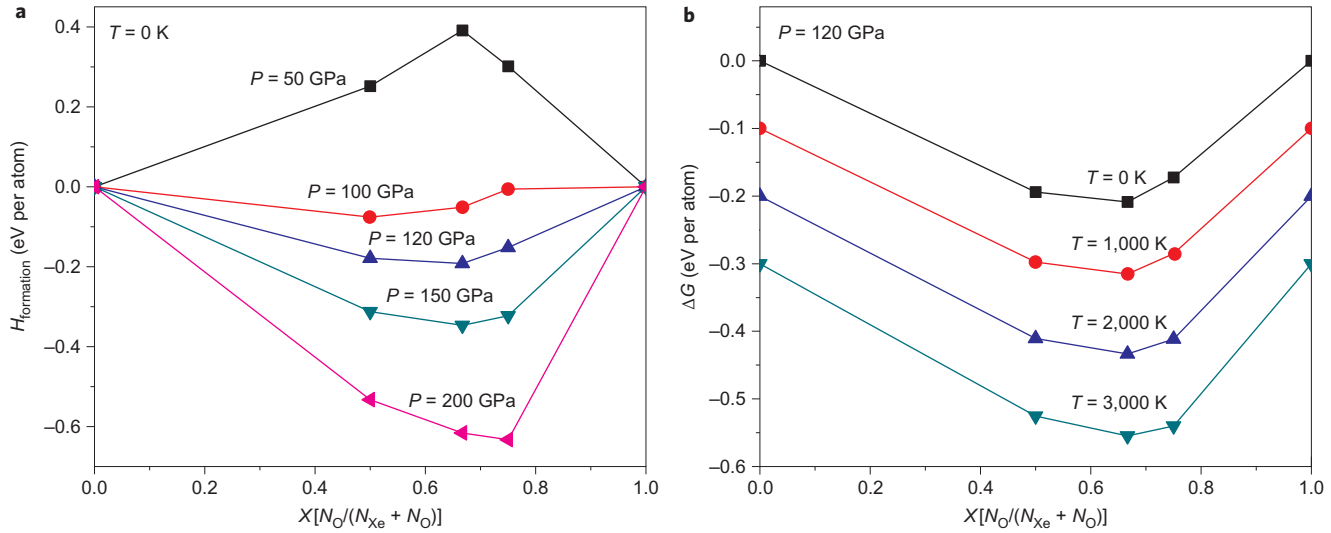

Figure 1 | Thermal stability of Xe–O compounds. a, Predicted formation enthalpy of Xe–O compounds at high P and $T = 0$ K. **b**, Predicted Gibbs free energy of formation of Xe–O compounds at different temperatures and $P = 120$ GPa. The compounds shown are (left to right) Xe, XeO, XeO_2, XeO_3 and O. For oxygen, the structures of the ζ-phase[36] and ε-phase[37] were used. For xenon, the face-centred cubic (fcc)[38] and hexagonal close-packed (hcp)[39] structures were considered, and hcp was found energetically more favourable above 100 GPa, in agreement with experiments[40]. For clarity, the Gibbs free energies of formation in **b** were shifted by −0.1, −0.2 and −0.3 eV/atom at 1,000, 2,000 and 3,000 K, respectively.

xenon atoms are in a twofold (linear) coordination and the Xe–O bonds form chains, with O–Xe–O angles of 175.6° and Xe–O–Xe angles of 112.6°. The alternating Xe–O bond lengths are 2.0 and 2.1 Å. The ELF picture (Fig. 2a) shows a toroidal maximum of ELF around each xenon atom, exactly what one should expect for the Xe^{2+} state. Above 145 GPa, XeO undergoes a phase transformation and forms a structure with the space group $P2_1/m$. In this structure there are two different environments for the Xe atoms (Xe1 and Xe2); Xe1 atoms connect to four oxygen atoms and have a square coordination, forming the same chains as in XeO_2 (suggesting that Xe1 atoms are in the tetravalent Xe^{4+} state). However, Xe2 can be described as neutral and not bonded to other atoms by any significant bonds. The presence of neutral non-bonded atoms in this structure is energetically favourable as it increases the packing density.

In XeO_2, the stable structure above 102 GPa has space group $P2_1/c$ and 24 atoms in the unit cell. The xenon atoms have a slightly non-planar square coordination and the structure consists of one-dimensional ribbons of edge-sharing XeO_4 squares (Xe–O distances of 2.0 and 2.1 Å), with four Xe–O bonds and two lone-pair ELF maxima forming an octahedron, as in the ambient-pressure metastable phase[8]. Just as in XeO, there are no peaks visible in the ELF isosurface along the Xe–O bonds (Fig. 2b). Above 198 GPa XeO_2–$P2_1/c$ transforms into the XeO_2–*Cmcm* structure. This non-trivial structure can be represented as having parallel zigzag xenon chains (Xe–Xe distances of 2.62 Å), with each xenon atom having two neighbouring oxygen atoms in the form of bent XeO_2 molecules (Xe–O distance of 1.95 Å; O–Xe–O angle of 160.7 Å).

XeO_3 becomes stable at 114 GPa. Its structure has space group $P4_2/mnm$ and 16 atoms in the unit cell. It is stable against decomposition into Xe and O_2, as well as into XeO or XeO_2 and O_2. As shown in the Supplementary Fig. S3a,b, the $P4_2/mnm$–XeO_3 structure is composed of two sublattices: square XeO_2 chains, suggesting the Xe^{4+} states, and linear chains made of O_2 dumbbells. Above 145 GPa, a new phase is formed where the molecules in the linear $–O_2–O_2–$ chains are partly dissociated and we observe the $–O_2–O–$ chain in the $C2/c$ phase with 48 atoms per unit cell (Supplementary Fig. S3c). Above 198 GPa, the structure transforms into a *Pmmn* phase with eight atoms per unit cell. In this remarkable structure, oxygen atoms form anticuboctahedra around the xenon atoms (Fig. 2c). The ELF distribution around xenon atoms in the *Pmmn* phase is spherical, which points to the Xe^{6+} valence state with a spherically symmetric $5s^2$ valence shell. Clearly, detailed analysis of the ELF distribution confirms the tendency to increasing oxidation states under pressure.

Xenon fluorides are stable under ambient conditions, xenon oxides become stable above 83 GPa, and xenon carbides are unstable at the very least up to 200 GPa (ref. 13). It thus appears that xenon forms compounds most readily with the most electronegative atoms, which in turn suggests that ionicity is essential. This is somewhat counterintuitive, given that the xenon atom has a very stable closed valence shell and its ionization potential and electronegativity are rather high. The electronegativity difference (1.4 for Xe–F, 0.8 for Xe–O and 0.56 for Xe–C) determines the degree of ionicity under ambient conditions. However, ionicity can be enhanced under pressure. Indeed, spontaneous ionization under pressure was recently found even in an element—boron[19].

To obtain further chemical insight into these exotic xenon oxides, we selected some of the stable structures containing Xe^{2+}, Xe^{4+} and Xe^{6+}, namely, XeO–*Pbcm* at 100 GPa, XeO_2–$P2_1/c$ at 150 GPa, and XeO_3–*Pmmn* at 200 GPa. Figure 3 shows the densities of states and their projection onto atomic orbitals for these structures. All of these xenon oxides are narrow-gap semiconductors. Using state-of-the-art GW calculations, we obtained the bandgaps: 1.52 eV for XeO–*Pbcm* at 100 GPa, 0.52 eV for XeO_2–$P2_1/c$ at 150 GPa, 0.15 eV for XeO_3–*Pmmn* at 200 GPa (these values should be accurate to within 5–10%).

The highest valence band levels are dominated by the *p*-orbitals of oxygen and xenon. Both the atom-projected densities of states and energy-decomposed electron densities suggest charge transfer from xenon to oxygen atoms. The contribution of the xenon *p*-orbitals decreases with increasing xenon oxidation number. The valence states dominated by *p* contributions in XeO–*Pbcm* contain about 40 electrons, with almost equal contributions from oxygen and xenon, namely 4.51 *p* electrons per xenon atom and 4.93 *p* electrons per oxygen atom. In the case of XeO_2–$P2_1/c$, there are about 112 such electrons, 31.94 from xenon and 80.16 from oxygen, or 3.99 *p* electrons per xenon and 5.01 *p* electrons per oxygen. This means that each xenon atom loses

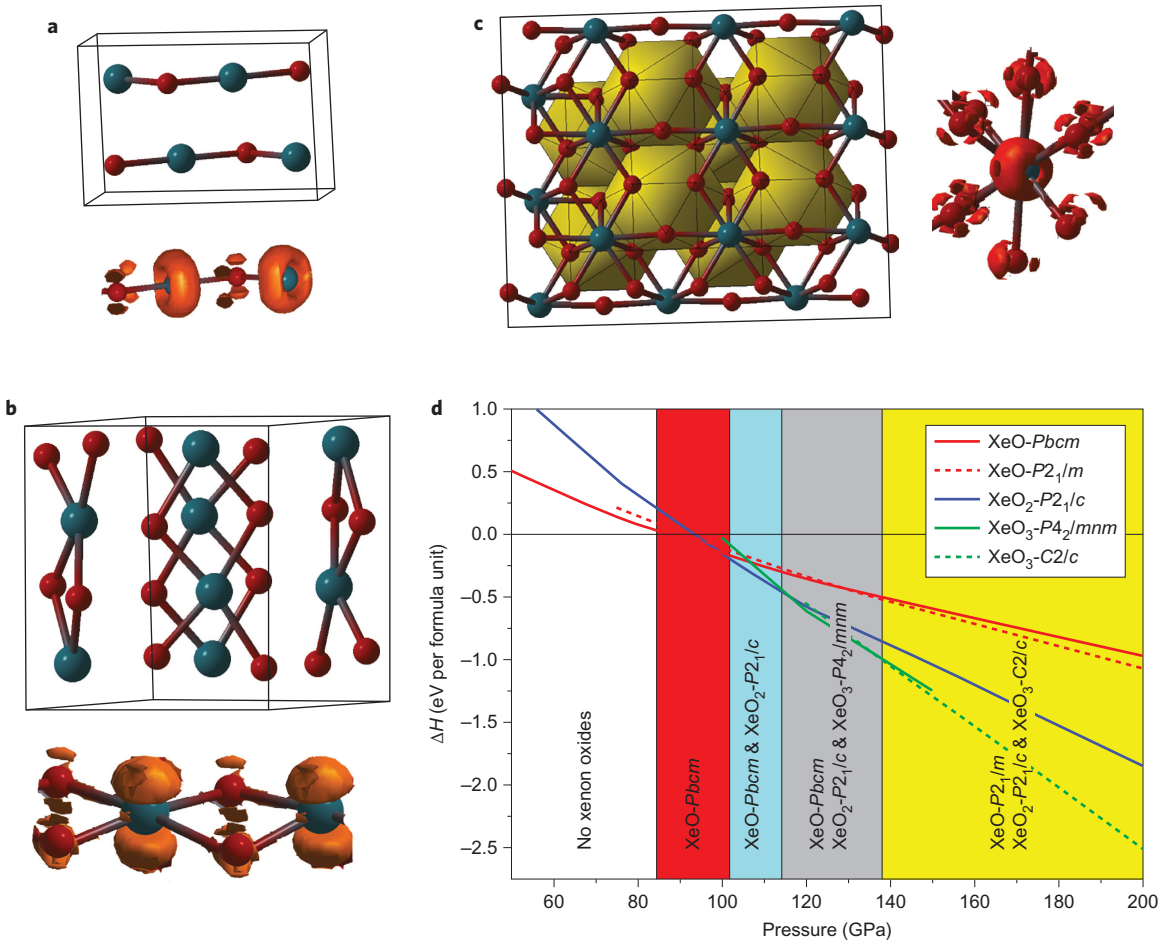

Figure 2 | Crystal structures, chemical bonding and stability range of Xe–O compounds. a, Crystal structure of XeO (*Pbcm*) at 100 GPa, and its ELF distribution (ELF = 0.85 isosurface) in the Xe–O chain. **b**, Crystal structure of XeO_2 ($P2_1/c$) at 120 GPa, and its ELF distribution (ELF = 0.85) in the chains of XeO_4 squares. **c**, Crystal structure of XeO_3 (*Pmmn*) at 200 GPa, and its ELF distribution (ELF = 0.82) in XeO_{12} anticuboctahedra. **d**, Enthalpies of formation of all stable xenon oxides are shown by lines. Stability fields are delineated by colours (at 198 GPa, $P2_1/c$ XeO_2 transforms to a *Cmcm* structure, and $C2/c$-XeO_3 transforms to the *Pmmn* phase, that is, just at the edge of the graph).

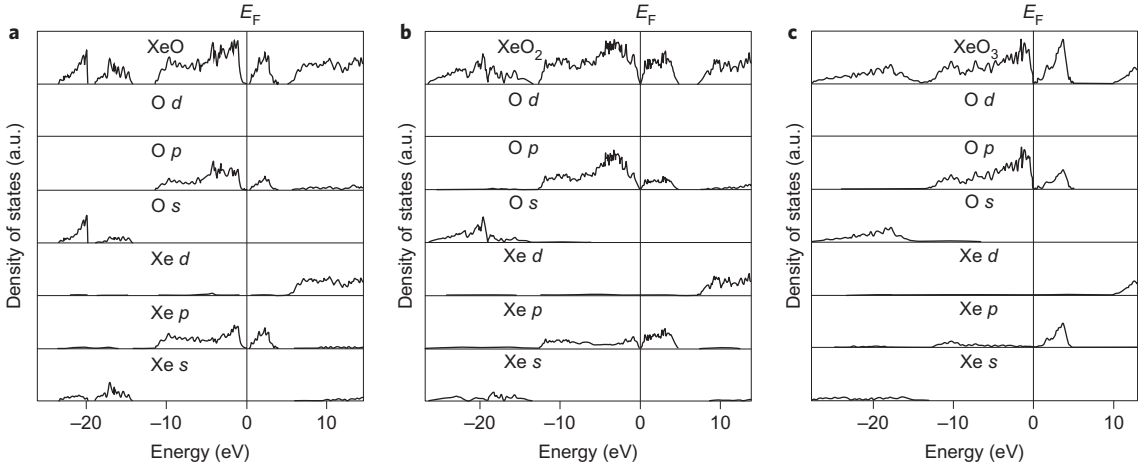

Figure 3 | Electronic structures of selected Xe–O compounds. a–c, Total and projected densities of states for XeO–*Pbcm* at 100 GPa (**a**), XeO_2–$P2_1/c$ at 150 GPa (**b**), XeO_3–*Pmmn* at 200 GPa (**c**). The sum over the plotted projections gives the total density of states for each system. The Fermi energy (E_F) is set as the highest valence band energy.

two *p* electrons, which are transferred into a *p* orbital of the oxygen atoms (each oxygen atom takes one *p* electron). Finally, in XeO_3–*Pmmn* there are about 36 electrons in the valence states dominated by *p* orbital contributions, 5.48 electrons from xenon and 30.10 from oxygen, leading to a further lowering to 2.74 electrons on xenon *p* orbitals and again to ~5 electrons on oxygen *p* orbitals.

Charge transfer was also investigated using Bader's analysis of electron density[20]. For XeO–*Pbcm* the net charge on the xenon

Table 1 | Eigenvalues of the traceless quadrupole moment tensor from the atomic Bader integration.

System	μ_1	μ_2	μ_3
XeO	−3.49	−2.04	5.53
XeO_2-Xe1	−5.50	1.83	3.67
XeO_2-Xe2	−5.90	2.33	3.57
XeO_3	−0.38	0.21	0.36

The selected xenon oxide structures are XeO–*Pbcm* at 100 GPa, XeO_2–$P2_1/c$ at 150 GPa, and XeO_3–*Pmmn* at 200 GPa.

atoms is 1.01, but it increases to 1.995, on average, in XeO_2–$P2_1/c$ and to 2.754 in XeO_3–*Pmmn*. Note that the net charge on the oxygen atoms stays almost the same in all three compounds and is very close to –1. This corresponds to an ionicity of ∼50%. Note that the charge transfer described by Bader analysis of an observable function, the electron density, confirms that found using orbital-projected density of states, a totally independent approach.

Bader analysis yields not only the net atomic charges, but also more subtle characteristics, such as the traceless quadrupole moment tensor $Q(\Omega)$, whose three eigenvalues μ_i $(i = 1,3)$ provide a good quantitative indicator of the departure of an atomic basin from sphericity. The eigenvectors associated with the eigenvalues μ_i give the principal directions for relative charge accumulation and depletion. For a spherical distribution, eigenvalues μ_i are all equal to zero. A deviation from zero indicates asphericity: negative eigenvalues μ_i arise from an accumulation of charge in the direction associated with the corresponding eigenvector and at the expense of the directions associated with positive μ_i. Our calculation (Table 1) shows that the xenon atoms in XeO_3–*Pmmn* are definitely more spherical, with eigenvalues μ_i all close to zero and about one order of magnitude lower than those for XeO_2 and XeO. This agrees with the ELF picture while also providing a quantitative measure of asphericity. XeO–*Pbcm* (with one *p* orbital partially empty) has, in agreement with the orbital picture, one direction of relative charge depletion (associated with μ_3) and two directions of unequal relative charge accumulation (associated with μ_1 and μ_2). Finally, in XeO_2–$P2_1/c$ there is one direction of relative charge accumulation (associated with μ_1) and two of unequal relative charge depletion (associated with μ_2 and μ_3), in agreement with the picture of two (partially) empty *p* orbitals.

High oxidation states, together with the high electronegativity of xenon, imply strong oxidative properties for xenon oxides. How likely is it that xenon oxides (or silicates) could exist in the Earth's lower mantle, thus explaining the missing xenon paradox? As discussed above, xenon oxides are only stable above 83 GPa, that is, at pressures corresponding to the lower mantle, where metallic iron should be present and the environment is strongly reducing[21,22]. The predicted xenon oxides are very strong oxidants and our calculations show that they will be reduced by iron, producing iron oxide and free xenon. We thus turned to the exploration of xenon silicates, focusing on $XeSiO_3$ and Xe_2SiO_4, which contain the least oxidized xenon. However, these, and all other investigated compositions, were unstable towards decomposition into XeO, XeO_2, SiO_2 and elemental xenon. We therefore conclude that, although xenon oxides are stable in the Xe–O system at pressures and temperatures of the Earth's lower mantle, in its strongly reducing environment neither silicates nor oxides of xenon can exist. Xenon silicates are unstable to decomposition, and xenon oxides will be reduced by metallic iron present in the lower mantle.

In summary, we have predicted the stability of xenon oxides at high pressure; indeed, this can be readily tested experimentally. With increasing pressure, increasingly high oxidation states of xenon will appear: first XeO (above 83 GPa), then XeO_2 (above 102 GPa) and XeO_3 (above 114 GPa). The present results clearly show that xenon loses its chemical inertness under pressure, and that charge transfer plays an essential role in the chemical bonding of xenon compounds, with their stability being strongly enhanced by electronegativity differences. Furthermore, pressure stabilizes the higher oxidation states of xenon atoms ($Xe^0 \rightarrow Xe^{2+} \rightarrow Xe^{4+} \rightarrow Xe^{6+}$) and enhances charge transfer from xenon to oxygen atoms. We find that xenon silicates are not stable at the pressures found in the Earth's mantle (<136 GPa) and that xenon oxides, although stable against decomposition into the elements, will be reduced to free xenon under the strongly reducing conditions of the lower mantle.

Although the formation of stable xenon oxides or silicates is not possible under the conditions found in the Earth's mantle, the formation of strong Xe–O bonds under pressure, clearly seen in our results, implies that xenon may still be retained at point or line defects or grain boundaries of mantle minerals. Xenon could also be stored in perovskite/post-perovskite stacking faults[23]. The facile chemical bonding between xenon and oxygen atoms demonstrated here and the preference of xenon atoms to terminate the silicate perovskite layers, observed in our simulations (see Supplementary Information), suggest this possibility. Indeed, the effect of trapping of trace elements by lattice defects is well known[24].

Methods

Crystal structure prediction. The evolutionary algorithm USPEX[15,16], used here for predicting new stable structures, searches for the structure with the lowest free energy at given pressure/temperature conditions and is capable of predicting the stable structure of a compound knowing just the chemical composition. Details of the method are described elsewhere[15,16] and a number of applications[13,16,19] illustrate its power. Structure relaxations were calculated using density functional theory (DFT) within the generalized gradient approximation (GGA)[25] in the framework of the all-electron projector augmented wave (PAW)[26] method as implemented in the VASP code[27]. We used a plane-wave kinetic energy cutoff of 520 eV, and the Brillouin zone was sampled with a resolution of $2\pi \times 0.07$ Å^{-1}, which showed excellent convergence of the energy differences, stress tensors and structural parameters. We studied systems containing up to 36 atoms per unit cell. The first generation of structures was created randomly. All structures were relaxed at constant pressure and 0 K and the enthalpy was used as fitness. The energetically worst structures (40%) were discarded and a new generation was created from the remaining structures through heredity, lattice mutation and permutation of atoms. The best structure of a generation was carried over into the next generation. We generally terminated the runs after 50 generations, and all runs had found the minimum-enthalpy structures much earlier. The population size was set to at least twice the number of atoms in the cell. Results obtained with and without the van der Waals functional[28] (as implemented in the VASP code) were very similar, and we show the results that include this functional. We explored the effects of temperature using the quasiharmonic approximation, for which phonon calculations were performed for all promising structures using the PHONOPY code[17]; for each structure, phonons were computed at ∼20–30 different volumes.

Chemical bonding analysis. The density of states and its projections onto atomic orbitals were calculated using the periodic linear combination of atomic orbitals (LCAO) approach, using the CRYSTAL-06 code[29] and the same DFT functional (GGA) as used in all calculations described here. Oxygen atoms were described by an 8–411+*d* all-electron basis set[30] and xenon atoms by a cc-pVTZ basis set[31], specifically devised for the fully relativistic ECP28MDF pseudopotential, with 26 electrons per xenon kept active. To avoid problems of numerical catastrophes[29], the original cc-157 pVTZ(12*s*11*p*9*d*1*f*)/ [5*s*4*p*3*d*1*f*] basis set[31] was slightly modified by removing the outermost *s*, *p* and *d* Gaussians and the *f* polarization function to yield a final (11*s*10*p*8*d*)/[5*s*4*p*3*d*] contracted basis set. The Kohn–Sham matrix was diagonalized on an isotropic 8 × 8 × 8 *k*-mesh, and the same mesh was used in the Fermi energy calculation and density matrix reconstruction. Bader's charges and atomic quadrupole moment tensors were evaluated from the periodic LCAO electron density and using the TOPOND package[32] interfaced to the CRYSTAL code. TOPOND determines the boundaries of the atomic basins and the integrated properties within these basins using fully analytical and on-the-fly evaluations of the electron density and its derivatives (up to fourth order); that is, no use is made of electron densities on a grid or of numerical approximations of electron density gradients[33]. Basin boundaries were determined using the PROMEGA algorithm[34], and the basin integration was performed in spherical coordinates, using Gaussian quadrature formulas. Bandgaps were calculated within the GW approximation as implemented in the VASP code[35]. We used the 12 × 6 × 10 *k*-points mesh for *Pbca*–XeO, 3 × 3 × 4 for $P2_1/c$–XeO_2, and 9 × 12 × 12 for *Pmmn*–XeO_3, respectively.

Received 5 March 2012; accepted 9 October 2012; published online 11 November 2012

References

1. Levy, H. A. & Agron, P. A. The crystal and molecular structure of xenon difluoride by neutron diffraction. *J. Am. Chem. Soc.* **85,** 241–242 (1963).
2. Templeton, D. H., Zalkin, A., Forrester, J. D. & Williamson, S. M. Crystal and molecular structure of xenon trioxide. *J. Am. Chem. Soc.* **85,** 817 (1963).
3. Hoyer, S., Emmler, T. & Seppelt, K. The structure of xenon hexafluoride in the solid state. *J. Fluor. Chem.* **127,** 1415–1422 (2006).
4. Kim, M., Debessai, M. & Yoo, C. S. Two- and three-dimensional extended solids and metallization of compressed XeF_2. *Nature Chem.* **2,** 784–788 (2010).
5. Somayazulu, M. *et al.* Pressure-induced bonding and compound formation in xenon hydrogen solids. *Nature Chem.* **2,** 50–53 (2010).
6. Smith, D. F. Xenon trioxide. *J. Am. Chem. Soc.* **85,** 816–817 (1963).
7. Selig, H., Claassen, H. H., Chernick C. L., Malm, J. G. & Huston, L. L. Xenon tetroxide: preparation and some properties. *Science* **143,** 1322–1323 (1964).
8. Brock, D. S. & Schrobilgen, G. J. Synthesis of the missing oxide of xenon, XeO_2, and its implications for Earth's missing xenon. *J. Am. Chem. Soc.* **133,** 6265–6269 (2011).
9. Grochala, W. Atypical compounds of gases, which have been called 'noble'. *Chem. Soc. Rev.* **36,** 1632–1655 (2007).
10. Anders, E. & Owen, T. Mars and Earth: origin and abundance of volatiles. *Science* **198,** 453–465 (1977).
11. Sanloup, C., Hemley, R. J. & Mao, H. K. Evidence for xenon silicates at high pressure and temperature. *Geophys. Res. Lett.* **29,** 1883–1886 (2002).
12. Sanloup, C. *et al.* Retention of xenon in quartz and Earth's missing xenon. *Science* **310,** 1174–1177 (2005).
13. Oganov, A. R., Ma, Y., Lyakhov, A. O., Valle, M. & Gatti, C. Evolutionary crystal structure prediction as a method for the discovery of minerals and materials. *Rev. Mineral. Geochem.* **71,** 271–298 (2010).
14. Caldwell, W. A. *et al.* Structure, bonding, and geochemistry of xenon at high pressures. *Science* **277,** 930–933 (1997).
15. Oganov, A. R. & Glass, C. W. Crystal structure prediction using *ab initio* evolutionary techniques: principles and applications. *J. Chem. Phys.* **124,** 244704 (2006).
16. Oganov, A. R., Lyakhov, A. O. & Valle, M. How evolutionary crystal structure prediction works—and why. *Acc. Chem. Res.* **44,** 227–237 (2011).
17. Togo, A., Oba, F. & Tanaka, I. First-principles calculations of the ferroelastic transition between rutile-type and $CaCl_2$-type SiO_2 at high pressures. *Phys. Rev. B* **78,** 134106 (2008).
18. Becke, A. D. & Edgecombe, K. E. A simple measure of electron localization in atomic and molecular systems. *J. Chem. Phys.* **92,** 5397–5403 (1990).
19. Oganov, A. R. *et al.* Ionic high-pressure form of elemental boron. *Nature* **457,** 863–867 (2009).
20. Bader, R. F. W. *Atoms in Molecules—A Quantum Theory* (Oxford Univ. Press, 1990).
21. Frost, J. C. *et al.* Experimental evidence for the existence of iron-rich metal in the Earth's lower mantle. *Nature* **428,** 409–412 (2004).
22. Zhang, F. & Oganov, A. R. Valence state and spin transitions of iron in Earth's mantle silicates. *Earth Planet. Sci. Lett.* **249,** 436–443 (2006).
23. Oganov, A. R., Martonak, R., Laio, A., Raiteri, R. & Parrinello, M. Anisotropy of Earth's D″ layer and stacking faults in the $MgSiO_3$ post-perovskite phase. *Nature* **438,** 1142–1144 (2005).
24. Urusov, V. S. & Dudnikova, V. B. The trace-component trapping effect: experimental evidence, theoretical interpretation, and geochemical applications. *Geochim. Cosmochim. Acta* **62,** 1233–1240 (1998).
25. Perdew, J. P., Burke, K. & Ernzerhof, M. Generalized gradient approximation made simple. *Phys. Rev. Lett.* **78,** 3865–3868 (1996).
26. Blochl, P. E. Projector augmented-wave method. *Phys. Rev. B* **50,** 17953–17979 (1994).
27. Kresse, G. & Furthmuller, J. Efficiency of *ab initio* total energy calculations for metals and semiconductors using a plane-wave basis set. *Phys. Rev. B* **54,** 11169–11186 (1996).
28. Klimes, J., Bowler, D. R. & Michaelides, A. Van der Waals density functionals applied to solids. *Phys. Rev. B* **83,** 195131 (2011).
29. Dovesi, R. *et al. CRYSTAL06 User's Manual* (University of Torino, 2006).
30. Towler, M. D. *et al. Ab initio* study of MnO and NiO. *Phys. Rev. B* **50,** 5041–5054 (1994).
31. Peterson, K. A. *et al.* Systematically convergent basis sets with relativistic pseudopotentials. II. Small-core pseudopotentials and correlation consistent basis sets for the post-*d* group 16–18 elements. *J. Chem. Phys.* **119,** 11113–11123 (2003).
32. Gatti, C. *TOPOND-98: An Electron Density Topological Program for Systems Periodic in N (N = 0–3) Dimensions* (CNR-ISTM, 1999).
33. Gatti, C. in *The Quantum Theory of Atoms in Molecules* (eds Matta, C.F. & Boyd, R.J.) 165–206 (Wiley-VCH, 2007).
34. Keith, T. *Molecules in Magnetic Fields*. PhD thesis, McMaster Univ. (1993).
35. Shishkin, M. & Kresse, G. Self-consistent *GW* calculations for semiconductors and insulators. *Phys. Rev. B* **75,** 235102 (2007).
36. Ma, Y., Oganov, A. R. & Glass, C. W. Structure of the metallic ζ-phase of oxygen and isosymmetric nature of ζ–ϵ phase transition: *ab initio* simulations. *Phys. Rev. B* **76,** 064101 (2007).
37. Lundegaard, L. F., Weck, G., McMahon, M. I., Desgreniers, S. & Loubeyre, P. Observation of an O_8 molecular lattice in the ε phase of solid oxygen. *Nature* **443,** 201–204 (2006).
38. Sears, D. R. & Klug, H. P. Density and expansivity of solid xenon. *J. Chem. Phys.* **37,** 3002–3006 (1962).
39. Sonnenblick, Y., Alexander, E., Kalman, Z. & Steinberger, I. Hexagonal close packed krypton and xenon. *Chem. Phys. Lett.* **52,** 276–278 (1977).
40. Boehler, R., Ross, M. & Boercker, D. B. High-pressure melting curves of alkali halides. *Phys. Rev. B* **53,** 556–563 (1996).

Acknowledgements

Calculations were performed on the CFN cluster and Blue Gene supercomputer (Brookhaven National Laboratory), Swiss Supercomputer Centre, Skif MSU supercomputer (Moscow State University) and at the Joint Supercomputer Center of the Russian Academy of Sciences (Moscow). A.R.O. thanks DARPA (grant no. W31P4Q1210008) and the National Science Foundation (grant no. EAR-1114313) for financial support.

Author contributions

A.R.O. designed the research. Q.Z. and D.Y.J. performed the calculations. Q.Z., D.Y.J., A.R.O. and C.G. interpreted data. A.O.L. and C.W.G. wrote the structure prediction code. Q.Z., D.Y.J., A.R.O. and C.G. wrote the manuscript.

Additional information

Supplementary information is available in the online version of the paper. Reprints and permission information is available online at http://www.nature.com/reprints. Correspondence and requests for materials should be addressed to Q.Z. and A.R.O.

Competing financial interests

The authors declare no competing financial interests.